4-1988

# Strain and Magnetic Fabric in Santa Catalina and Pinaleno Mountains Metamorphic- Core-Complexes Mylonite Zones, Arizona

Amy S. Ruf

Stephen J. Naruk

Robert F. Butler
*University of Portland*, butler@up.edu

Gary J. Calderone

STRAIN AND MAGNETIC FABRIC IN
THE SANTA CATALINA AND PINALENO
MOUNTAINS METAMORPHIC CORE COMPLEX
MYLONITE ZONES, ARIZONA

Amy S. Ruf, Stephen J. Naruk,[1]
Robert F. Butler, and Gary J. Calderone[2]

Department of Geosciences, University of Arizona,
Tucson

*Abstract.* Anisotropy of magnetic susceptibility
(AMS) is capable of recording finite strain in
weakly magnetized rocks. AMS was measured for
228 samples from 20 sites in two mylonite zones
with the same deformational history. AMS
measurements were compared with finite strains
determined from dike rotations and from foliation
orientations. In one zone (the Santa Catalina
Mountains) the orientations of susceptibility and
finite strain ellipsoids are in excellent agreement,
and there is a logarithmic relationship between
susceptibility difference ($\Delta K_i = [K_i-\overline{K}]/\overline{K}$) and
finite strain magnitude. In the second zone (the
Pinaleno Mountains) minimum susceptibility is
perpendicular to the finite flattening plane, but the
maximum susceptibility does not parallel the
maximum extension direction, and there is no
systematic relationship between susceptibility
magnitude and strain magnitude. Oriented polished
thin sections indicate that magnetite in the
protolith of the Santa Catalina mylonite occurs as
randomly oriented, elongate grains. With
subsequent deformation, the long axes are rotated
into the maximum extension direction. In the
Pinaleno mylonites, both equant and elongate
magnetite grains are present. With deformation,
the elongate magnetite grains are rotated into the
maximum flattening plane but show no preferred
orientation within this plane. AMS in the two
mylonite zones appears to be predominantly
controlled by the orientation of elongate magnetite
grains with respect to the megascopic fabric. The
final orientation of the elongate grains is a
function of their initial orientation as well as the
finite strain. Therefore, despite similar
deformational histories, the two zones display
different AMS patterns due to the differences in
occurrence, initial orientation, and shape of
ferromagnetic grains.

[1]Now at Shell Western E & P Inc., Houston,
Texas.
[2]Also at U.S. Geological Survey, Flagstaff,
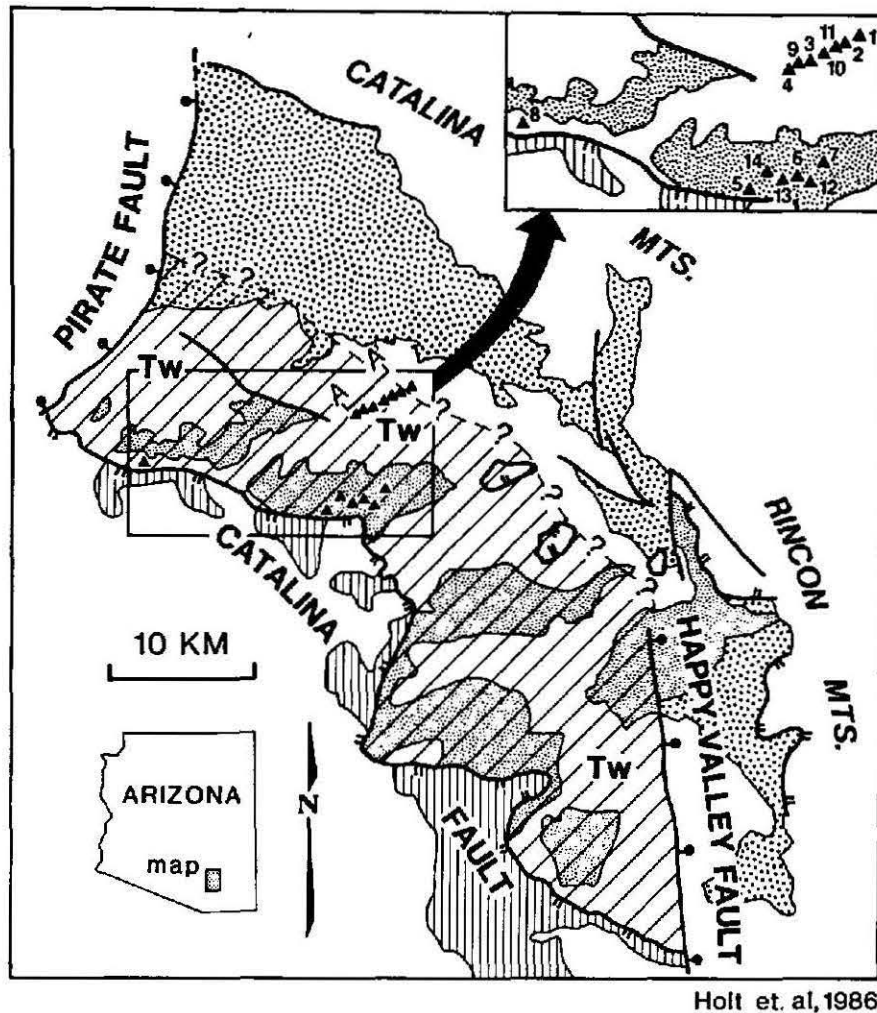Arizona.

INTRODUCTION

Both anisotropy of magnetic susceptibility (AMS)
and strain are second order tensors geometrically
represented by ellipsoids. Many recent
investigations of AMS and strain have established a
general coincidence of the principal axes of the
magnetic fabric and petrofabric ellipsoids, with the
maximum susceptibility axis oriented parallel to
petrographic lineation and the minimum
susceptibility axis oriented perpendicular to
foliation [Goldstein and Brown, 1986; Rathore, 1985;
Kligfield et al., 1983; Rathore et al., 1983] (and
review by Hrouda [1982]). Such studies have been
carried out in sedimentary rocks [e.g., Graham,
1966; Kligfield et al., 1977, 1982], igneous rocks
[e.g., Rathore, 1980, 1985], and metamorphic rocks

Holt et. al, 1986

penetratively mylonitized rocks of lower plate

upper-plate rocks

Tertiary plutonic and sedimentary rocks, Paleozoic, Cretaceous and late Precambrian sediments

Precambrian Oracle quartz monzonite intruded by Tw

⌣ fault      ⌣⌣⌣ detachment fault      •⌣•⌣ normal fault

Fig. 1a. Geologic map of the Santa Catalina-Rincon Mountains metamorphic core complex, showing AMS site locations (triangles). Tw, Wilderness granite. (Modified from Holt et al. [1986]).

[e.g., Goldstein, 1980; Goldstein and Brown, 1986]. This report discusses the applicability of AMS as a strain indicator in ductilely deformed granitic rocks in the mylonite zones of the Santa Catalina and Pinaleno Mountains metamorphic core complexes (Figure 1), two mylonite zones for which the deformational histories and finite strain values are known [Naruk, 1986a, b, 1987a, b].

Previous AMS studies have suggested that it is possible to obtain complete strain ellipsoid data from the magnetic susceptibility ellipsoid, which can be measured rapidly and accurately [Goldstein

and Brown, 1986; Rathore et al., 1983; Goldstein, 1980]. However, in none of these studies has detailed strain control such as that included in the present study been available. This research was initiated with two particular goals in mind: (1) to characterize strain in the mylonite zones in terms of AMS data and (2) to examine the development of magnetic anisotropy in the mylonite zones with increasing strain.

The Santa Catalina and Pinaleno Mountains are two of approximately 25 North American mountain ranges identified as Cordilleran metamorphic core

Fig. 1b. Geologic map of the Pinaleno Mountains mylonite zone, showing AMS site locations (PN1-PN6).

complexes [Davis and Coney, 1979; Crittenden et al., 1980]. The mylonite zones of both the Santa Catalina and Pinaleno Mountains are low-dipping, nor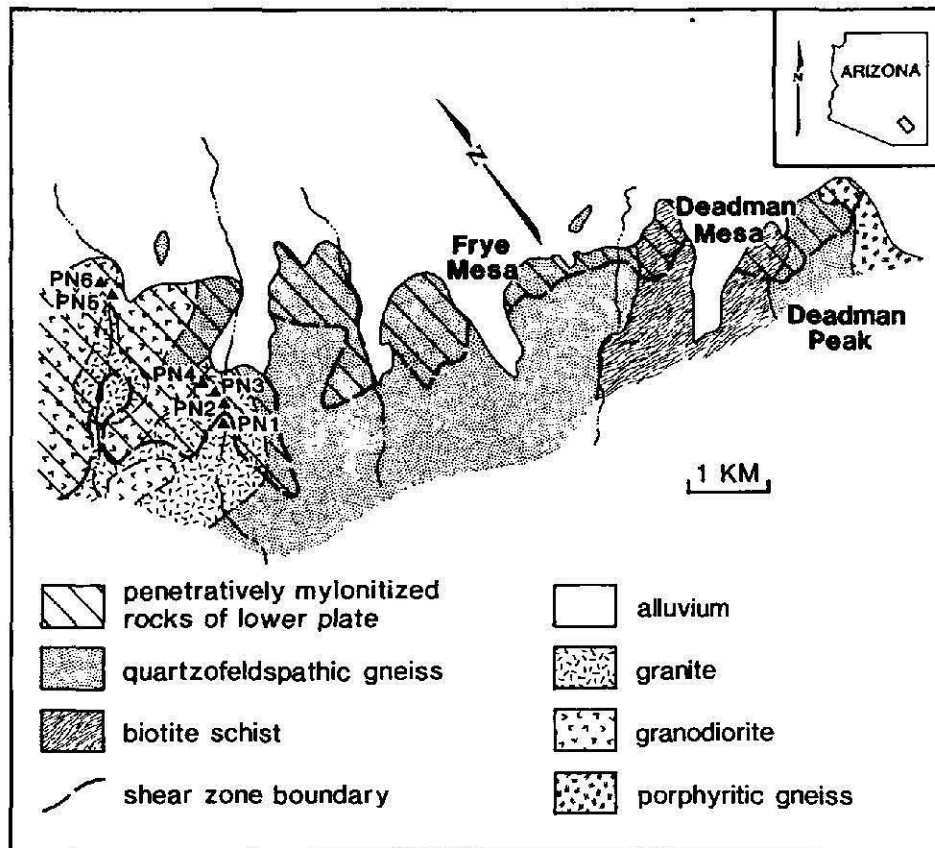mal displacement zones of pervasively foliated and lineated s-c (foliated with shear bands) mylonites. The lower boundaries of both zones are gradational contacts between the mylonites and their undeformed granitic equivalents. These transitions between undeformed rocks and mylonites provide a significant strain gradient within which to examine the development of magnetic anisotropy (Figure 2). Furthermore, the finite strains and deformational histories of these zones are already known in significant detail [Naruk, 1986a, b, 1987a, b], thus providing the basis for a controlled comparison of AMS and strain data.

## STRAIN DETERMINATIONS

Both the Santa Catalina and Pinaleno mylonite zones are zones of simple shear deformation, and both have well-defined planar lower boundaries. In both zones the mylonitic foliation surfaces are discordant to the zone boundary and parallel to the XY surface of the finite strain ellipsoid (axes $X \geq Y \geq Z$) [Naruk, 1986a, b, 1987a, b].

The Santa Catalina zone cuts across and displaces a suite of petrologically distinct dikes. These dikes have a uniform orientation in the undeformed state, as well as uniform, but different, orientations in the deformed state. The shear strain ($\gamma$) within the Santa Catalina zone is related to the orientation of these dikes by the following equation [Ramsay, 1967] (see Figure 3):

$$\gamma = \cot \alpha' - \cot \alpha \tag{1}$$

where

$$\gamma = \tan \psi$$

and

$$\psi = \text{angular shear}$$

$\alpha'$ = the angle, measured in the XZ plane, between the deformed dike and the shear zone boundary, and $\alpha$ = the angle, also measured in the XZ plane, between the undeformed dike and the shear zone boundary.

In simple shear, the XY plane of the finite strain ellipsoid rotates as a function of shear strain magnitude. Specifically, the angle ($\theta'$) between the XY plane and the shear zone boundary is an inverse function of the shear strain [Ramsay and Graham, 1970]:
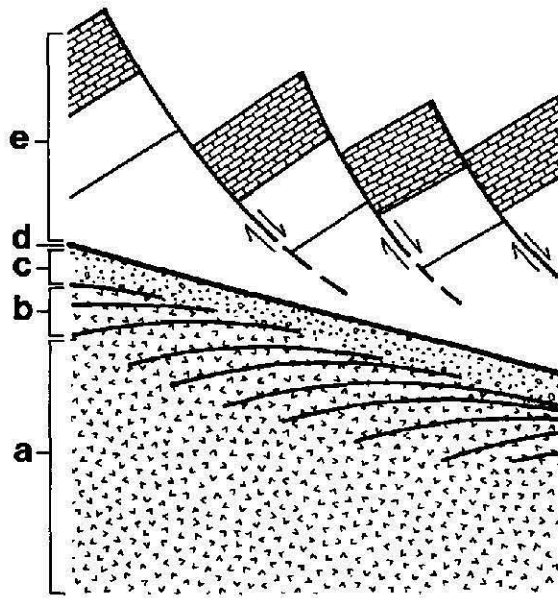
Fig. 2. Schematic diagram of a metamorphic core complex. (a) nonmylonitic core, (b) mylonite zone, (c) altered breccias, (d) detachment fault, (e) brittlely extended upper plate. The transition from Figure 2a to 2b represents a significant strain gradient from essentially undeformed rocks to their mylonitic equivalents. This gradient provides the basis for a controlled comparison of AMS and strain data.

$$\gamma = 2 \cot (2\theta') \qquad (2)$$

Thus, where the orientation of the XY surface is known, $\gamma$ can be calculated directly from (2). Alternatively, where $\gamma$ is known, $\theta'$ can be calculated from (2).

Where dikes outcrop in the Santa Catalina zone, $\gamma$ can be calculated from (1), and $\theta'$ can be calculated from (2). The resultant values of $\theta'$ equal the observed angles between the foliation surfaces and the shear zone boundary. This implies that the foliation surfaces represent the finite XY surface and that $\gamma$ can be calculated directly from (2), substituting the measured angle between the foliation and the shear zone boundary for $\theta'$.

The Pinaleno mylonite zone cuts across and displaces lithologic contacts in metamorphic rocks. The changes in orientations of these contacts were used to calculate $\gamma$ from (1) and $\theta'$ from (2), exactly as in the Santa Catalina zone. As in the Santa Catalina zone, the resultant $\theta'$ values equal the measured angles between the foliation surfaces and the shear zone boundary. This again implies that the foliation surfaces represent the finite XY surface and that the angles between the foliation and the shear zone boundary represent $\theta'$. Thus, at sites with planar markers, $\gamma$ was calculated from (1). At sites without such markers, $\gamma$ was calculated from (2), substituting the measured

angles between the foliation and the shear zone boundary for $\theta'$ (see Table 1).

FIELD AND LABORATORY METHODS FOR AMS MEASUREMENT

In both areas, samples for AMS measurement were collected from undeformed granite and from deformed granite, with each of the deformed sites representing a different degree of strain. In the Santa Catalina zone in particular, samples were collected from one site in undeformed granite
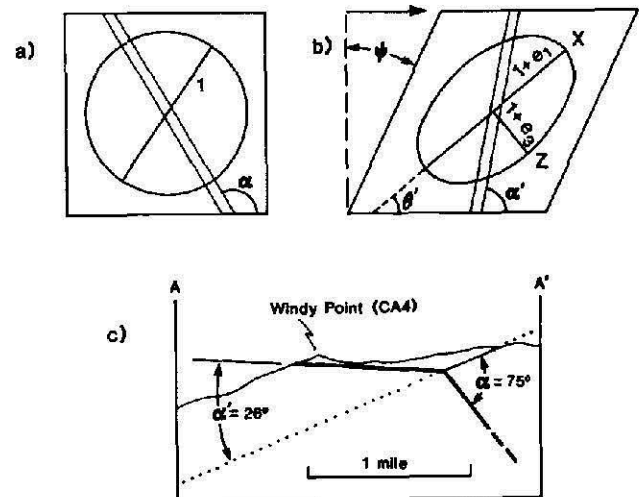


Fig. 3. Schematic block diagrams of simple shear strain equations. No strain occurs perpendicular to the plane of the figure ($e_y = 0$). (a) Undeformed state. The strain ellipse is represented by the circle with radius 1. The planar marker makes an angle $\alpha$ with the edge of the cube. (b) Deformed state, after simple shear of $\gamma$ (= $\tan \psi$, where $\gamma$ = shear strain and $\psi$ = angular shear) parallel to the edge of the cube. The circle becomes an ellipse with major and minor axes of $1 + e_1$ and $1 + e_3$, respectively. The major axis is oriented at an angle $\theta'$ to the edge of the cube. The planar marker is oriented at an angle $\alpha'$ to the edge of the cube. These angles are related to shear strain ($\gamma$) by

$$\gamma = \cot \alpha' - \cot \alpha \qquad (1)$$

$$\gamma = 2\cot 2\theta' \qquad (2)$$

(c) Cross section parallel to lineation across the boundary of the Santa Catalina Mountains mylonite zone (no vertical exaggeration, location shown in Figure 1a). At sites CA3 and CA4, $\gamma$ was calculated from changes in dike orientations (from $\alpha$ to $\alpha'$) using (1). The values of $\gamma$ calculated from (1) equal the values of $\gamma$ calculated from (2), assuming that the mylonitic foliation (S surfaces) equals the XY strain plane. Equation (2) was subsequently used to calculate $\gamma$ values at sites CA5-CA14, where independent markers such as dikes or contacts are not available.

TABLE 1. AMS and Strain Data for the Santa Catalina (CA) and Pinaleno Mountains (PN) Mylonite Zones

| Site | Inclination, deg | Declination, deg | $K_1$ | $K_2$ | $K_3$ | $K_{mean}$ | $\Delta K_1$ | $\Delta K_2$ | $\Delta K_3$ | K | $\theta'$ | $\gamma$ | $1+e_1$ | $1+e_3$ |
|---|---|---|---|---|---|---|---|---|---|---|---|---|---|---|
| CA1 | 33.1 | 6.2 | 0.143 | 0.108 | 0.098 | 0.116 | 0.233 | -0.075 | -0.158 | 1.001 | - | ~ | 1.00 | 1.00 |
| CA2 | 5.0 | 219.3 | 0.275 | 0.246 | 0.226 | 0.249 | 0.104 | -0.012 | -0.092 | 1.028 | - | ~ | - | - |
| CA3 | 4.7 | 43.8 | 0.135 | 0.118 | 0.115 | 0.123 | 0.097 | -0.039 | -0.058 | 1.003 | 30.0 | 1.1 | 1.73 | 0.58 |
| CA4 | 6.8 | 49.2 | 0.653 | 0.571 | 0.481 | 0.568 | 0.148 | 0.000 | -0.154 | 0.991 | 23.0 | 1.9 | 2.36 | 0.42 |
| CA5 | 3.8 | 241.3 | 12.179 | 10.348 | 8.634 | 10.348 | 0.180 | 0.000 | -0.170 | 0.959 | 12.0 | 4.5 | 4.70 | 0.21 |
| CA6 | 2.4 | 225.6 | 0.127 | 0.113 | 0.100 | 0.114 | 0.120 | 0.000 | -0.110 | 0.991 | 14.0 | 3.8 | 4.01 | 0.25 |
| CA7 | 11.4 | 238.8 | 1.497 | 1.258 | 0.900 | 1.218 | 0.230 | 0.030 | -0.260 | 0.849 | 15.0 | 3.5 | 3.73 | 0.27 |
| CA8 | 16.0 | 236.9 | 0.872 | 0.710 | 0.583 | 0.722 | 0.210 | -0.020 | -0.190 | 1.008 | 9.5 | 5.8 | 5.98 | 0.16 |
| CA9 | 0.6 | 46.7 | 0.439 | 0.358 | 0.304 | 0.367 | 0.190 | -0.020 | -0.170 | 1.018 | 23.0 | 2.0 | 2.41 | 0.41 |
| CA10 | 4.5 | 45.6 | 0.540 | 0.469 | 0.391 | 0.467 | 0.160 | 0.000 | -0.160 | 0.958 | 30.0 | 1.2 | 1.75 | 0.57 |
| CA11 | 7.5 | 38.4 | 1.087 | 1.032 | 0.967 | 1.028 | 0.060 | 0.000 | -0.060 | 0.963 | 27.0 | 1.5 | 1.97 | 0.50 |
| CA12 | 0.7 | 57.9 | 1.605 | 1.368 | 1.183 | 1.385 | 0.160 | -0.010 | -0.150 | 1.007 | 14.0 | 3.8 | 4.14 | 0.24 |
| CA13 | 2.0 | 230.1 | 0.579 | 0.543 | 0.482 | 0.534 | 0.080 | 0.020 | -0.100 | 0.938 | 17.0 | 3.0 | 3.29 | 0.31 |
| CA14 | 12.6 | 242.6 | 7.904 | 5.922 | 4.505 | 6.113 | 0.290 | -0.030 | -0.260 | 1.015 | 24.0 | 1.8 | 2.25 | 0.45 |
| PN1 | 8.1 | 50.4 | 5.063 | 4.625 | 3.996 | 4.561 | 0.110 | 0.014 | -0.124 | 0.947 | - | - | 1.00 | 1.00 |
| PN2 | 20.8 | 337.8 | 2.237 | 2.173 | 1.926 | 2.109 | 0.060 | 0.030 | -0.090 | 0.921 | 8.0 | 2.8 | 3.08 | 0.32 |
| PN3 | 12.6 | 43.2 | 0.169 | 0.163 | 0.152 | 0.162 | 0.046 | 0.012 | -0.058 | 1.028 | 17.0 | 3.0 | 3.27 | 0.31 |
| PN4 | 21.7 | 60.3 | 6.265 | 5.636 | 4.872 | 5.588 | 0.121 | 0.008 | -0.129 | 0.965 | 18.0 | 2.8 | 3.08 | 0.32 |
| PN5 | 13.7 | 46.7 | 0.673 | 0.622 | 0.541 | 0.634 | 0.099 | 0.016 | -0.115 | 0.955 | 21.0 | 2.2 | 2.61 | 0.38 |
| PN6 | 8.9 | 61.4 | 0.820 | 0.772 | 0.662 | 0.751 | 0.091 | 0.028 | -0.119 | 0.922 | 25.0 | 1.7 | 2.14 | 0.47 |

Inclination and declination are the mean inclination and declination, respectively, for the maximum susceptibility at each site; $K_1$, $K_2$, and $K_3$ ($1 \geq 2 \geq 3$) are the mean principal susceptibility magnitudes (SI units) at every site, and $K_{mean}$ is the mean susceptibility for every site; $\Delta K_1$, $\Delta K_2$, and $\Delta K_3$ ($1 \geq 2 \geq 3$) are the principal susceptibility differences at each site; K, the magnetic anisotropy factor, is $(K_1/K_2)/(K_2/K_3)$; $1 + e_1$ and $1 + e_3$ are the principal elongation and principal flattening values for each site, respectively; $\gamma$ is the shear strain, and $\theta'$ is as portrayed in Figure 3b.

(CA1) and from 13 sites in deformed granite (CA2-CA14). The strain in the deformed granite ranges from $(X/Z) = 3$ ($\gamma = 1.1$) to $(X/Z) = 36$ ($\gamma = 5.8$). In the Pinaleno zone, samples were collected from one site in essentially undeformed granite (PN1), and from five sites in deformed granite and granodiorite (PN2-PN6). The strains in the deformed samples range from $\gamma = 1.7$ to $\gamma = 3.0$. Nine to 15 oriented core samples of 2.54 cm (1") diameter were collected at each site using a portable drill. Core orientations were made using a sun compass and a Brunton compass for azimuthal orientation and an inclinometer for dip determination. Duplicate sun compass and Brunton compass determinations of core azimuths were within ± 2°, indicating no significant deflections of the magnetic compass from the expected local declination.

Each core sample was cut into a 1- to 2.5-cm-length cylindrical specimen. Low-field magnetic susceptibility of each specimen was measured on a SAPPHIRE SI-2 susceptibility bridge. Each specimen was measured along 12 axes with two separate measurements for each axis. This procedure allows determination of magnitude and direction of the principal susceptibilities as well as an estimate of the bulk susceptibility.

Oriented and polished thin sections were prepared from field-oriented block samples of unstrained granite (sites CA1 and PN1), moderately strained mylonite (sites CA3 and PN2), and highly strained mylonite (sites CA8 and PN3). Three thin sections were cut from each sample parallel to the three principal finite strain planes. The thin sections were analyzed in reflected and transmitted light for the identity, size, shape, and orientation of the magnetic minerals.

## RESULTS

### Santa Catalina Mountains

The results of AMS measurements and strain determinations for each site in the Santa Catalina Mountains are summarized in Tables 1 and 2. For each individual sample, direction and magnitude of

TABLE 2.  Average Directions of Strain Indicators and AMS Axes

| Site | Average Direction of Lineation | | | | | | Average Direction of $K_1$ | | | | | |
| | Incli-nation, deg | Decli-nation, deg | $\alpha_{95}$, deg | N | R | k | Incli-nation, deg | Decli-nation, deg | $\alpha_{95}$, deg | N | R | k |
|---|---|---|---|---|---|---|---|---|---|---|---|---|
| CA1 | No structural data | | | | | | 33.1 | 6.2 | 40.1 | 12 | 6.86 | 2.14 |
| CA2 | No structural data | | | | | | 5.0 | 219.3 | 28.5 | 11 | 8.16 | 3.53 |
| CA3 | 11.3 | 26.1 | 32.2 | 12 | 8.04 | 2.78 | 4.7 | 43.8 | 24.7 | 11 | 8.72 | 4.39 |
| CA4 | 5.9 | 42.5 | 22.9 | 32 | 18.02 | 2.22 | 6.8 | 49.2 | 9.8 | 13 | 12.35 | 18.68 |
| CA5 | 10.3 | 244.7 | 3.2 | 6 | 5.99 | 442.75 | 3.8 | 241.3 | 4.9 | 12 | 11.86 | 80.17 |
| CA6 | 3.0 | 245.0 | 3.0 | 3 | 3.00 | 1641.61 | 2.4 | 225.6 | 28.3 | 11 | 8.20 | 3.57 |
| CA7 | 10.3 | 245.0 | 5.0 | 4 | 3.99 | 344.72 | 11.4 | 238.8 | 12.3 | 11 | 10.32 | 14.73 |
| CA8 | 17.3 | 240.0 | 6.0 | · 4 | 3.99 | 233.20 | 16.0 | 236.9 | 8.9 | 10 | 9.70 | 30.45 |
| CA9 | 3.0 | 32.5 | - | 2 | 2.00 | - | 0.6 | 46.7 | 12.1 | 12 | 11.20 | 13.81 |
| CA10 | 12.3 | 26.8 | 9.1 | 4 | 3.97 | 101.87 | 4.5 | 45.6 | 4.5 | 14 | 13.83 | 80.08 |
| CA11 | 4.8 | 30.5 | 9.4 | 4 | 3.97 | 97.24 | 7.5 | 38.4 | 37.6 | 11 | 6.90 | 2.44 |
| CA12 | 6.0 | 239.0 | 1.5 | 3 | 3.00 | 6641.81 | 0.7 | 57.9 | 12.2 | 8 | 7.68 | 21.63 |
| CA13 | 3.1 | 242.0 | 3.0 | 7 | 6.98 | 399.98 | 2.0 | 230.1 | 9.9 | 9 | 8.71 | 27.97 |
| CA14 | 21.2 | 48.3 | 113.6 | 8 | 2.21 | 1.21 | 12.6 | 242.6 | 27.1 | 9 | 7.25 | 4.56 |
| PN1 | No structural data | | | | | | 8.1 | 50.4 | 19.0 | 10 | 8.79 | 7.44 |
| PN2 | 17.1 | 46.0 | 5.3 | 6 | 5.97 | 159.43 | 20.8 | 337.8 | 27.2 | 10 | 7.81 | 4.11 |
| PN3 | 22.5 | 44.5 | 2.6 | 6 | 5.99 | 689.44 | 12.6 | 43.2 | 20.9 | 10 | 8.57 | 6.31 |
| PN4 | 25.2 | 54.6 | 6.7 | 6 | 5.95 | 101.02 | 21.7 | 60.3 | 10.2 | 8 | 7.77 | 30.29 |
| PN5 | 19.5 | 40.0 | - | 2 | 1.99 | - | 13.7 | 46.7 | 25.2 | 10 | 8.06 | 4.63 |
| PN6 | 20.1 | 49.7 | 15.0 | 3 | 2.97 | 68.54 | 8.9 | 61.4 | 26.6 | 8 | 6.67 | 5.28 |

magnetic fabric are determined by the direction of the principal susceptibility axes and by the differences in susceptibility in those directions, respectively.  The principal susceptibility directions for each sample from four representative sites are shown in Figure 4.  Homogeneity of magnetic fabric within a particular site can be determined by the degree of clustering of the principal susceptibility axes from the multiple samples within the site.  In turn, this clustering can be quantified by use of Fisher's [1953] statistics for calculating site mean directions for each principal axis and attendant angular confidence intervals for these mean directions.  Table 2 provides a site-by-site comparison between the site mean AMS directions and site mean directions of strain indicators.

In the undeformed granite (CA1) there is no significant magnetic fabric.  The principal susceptibility directions are essentially randomly distributed; there is no well-defined clustering of either maximum, intermediate, or minimum susceptibility directions.  In site CA2 a prolate magnetic fabric has developed, resulting in well-defined maximum susceptibility axis directions.  The maximum susceptibility directions are

consistently oriented parallel to the maximum extension direction of the mylonite zone (approximately N40°E; see Table 2).  The intermediate and minimum directions lie in the plane perpendicular to the maximum susceptibility direction, but they are not isolated from each other.

In sites CA3 and CA4 the maximum, intermediate, and minimum susceptibilities have become increasingly isolated from each other.  In both CA3 and CA4 the maximum susceptibility direction parallels the mylonitic lineation direction (L), and the minimum susceptibility direction parallels the pole to the mylonitic foliation plane (F) (see Figure 5 and Table 2).  In general, the principal susceptibility directions from all sites (CA2-CA14) parallel the megascopic fabric elements of the mylonite zone; the maximum susceptibilities and the mylonitic lineation both dip gently to the northeast, and the minimum susceptibilities parallel the pole to the mylonitic foliation.

The magnetic anisotropy plot [Hrouda, 1982] (Figure 6) shows the anisotropy factor, K, of the susceptibility ellipsoids for the Santa Catalina sites (solid circles).  The anisotropy factor is equal to

TABLE 2. (Continued)

| Site | Average Direction of Foliation Pole | | | | | | Average Direction of $K_3$ | | | | | |
|------|-------------------------|--------------------------|--------------|----|-------|---------|-------------------------|--------------------------|--------------|----|-------|--------|
| | Incli-nation, deg | Decli-nation, deg | $\alpha_{95}$, deg | N | R | k | Incli-nation, deg | Decli-nation, deg | $\alpha_{95}$, deg | N | R | k |
| CA1 | No structural data | | | | | | 16.5 | 158.2 | 34.2 | 12 | 7.72 | 2.57 |
| CA2 | No structural data | | | | | | 18.1 | 133.6 | 25.9 | 11 | 8.55 | 4.08 |
| CA3 | 75.3 | 272.3 | 6.3 | 12 | 11.77 | 48.68 | 82.4 | 315.4 | 24.3 | 11 | 8.77 | 4.48 |
| CA4 | 83.7 | 285.4 | 2.2 | 30 | 29.79 | 140.68 | 78.9 | 291.6 | 7.1 | 13 | 12.65 | 35.15 |
| CA5 | 84.1 | 263.2 | 17.5 | 6 | 5.68 | 15.55 | 70.3 | 341.2 | 8.0 | 12 | 11.64 | 30.55 |
| CA6 | 61.0 | 338.4 | 3.4 | 3 | 3.00 | 1342.61 | 73.7 | 323.2 | 17.1 | 11 | 9.77 | 8.12 |
| CA7 | 72.8 | 198.2 | 7.2 | 4 | 3.98 | 163.67 | 67.3 | 355.6 | 5.1 | 11 | 10.87 | 79.07 |
| CA8 | 52.5 | 357.5 | 2.6 | 4 | 4.00 | 1215.27 | 47.1 | 345.3 | 4.4 | 10 | 9.93 | 123.70 |
| CA9 | 85.8 | 231.1 | 4.5 | 3 | 3.00 | 745.26 | 83.3 | 241.1 | 15.3 | 12 | 10.78 | 9.95 |
| CA10 | 75.3 | 248.0 | 10.6 | 4 | 3.96 | 76.51 | 79.2 | 291.1 | 6.1 | 14 | 13.70 | 43.60 |
| CA11 | 83.0 | 214.1 | 7.7 | 4 | 3.98 | 141.86 | 68.1 | 128.3 | 32.2 | 11 | 7.64 | 2.97 |
| CA12 | 79.0 | 189.2 | 4.3 | 3 | 3.00 | 838.11 | 74.5 | 318.3 | 12.9 | 8 | 7.64 | 19.31 |
| CA13 | 79.0 | 348.7 | 2.8 | 7 | 6.99 | 476.03 | 79.6 | 330.3 | 5.9 | 9 | 8.70 | 77.06 |
| CA14 | 75.9 | 310.6 | 12.5 | 8 | 7.66 | 20.48 | 75.7 | 9.8 | 9.4 | 9 | 8.74 | 31.14 |
| PN1 | No structural data | | | | | | 80.7 | 241.9 | 7.9 | 10 | 9.76 | 38.21 |
| PN2 | 78.1 | 236.1 | 14.4 | 6 | 5.78 | 22.69 | 69.5 | 181.4 | 5.1 | 10 | 9.90 | 89.24 |
| PN3 | 66.3 | 237.1 | 6.2 | 6 | 5.96 | 117.93 | 80.5 | 194.3 | 16.2 | 10 | 9.09 | 9.91 |
| PN4 | 65.0 | 236.6 | 4.3 | 6 | 5.98 | 244.04 | 61.0 | 198.3 | 6.7 | 8 | 7.90 | 69.80 |
| PN5 | 71.4 | 226.3 | 9.1 | 3 | 2.99 | 186.05 | 63.4 | 177.9 | 20.0 | 10 | 8.67 | 6.78 |
| PN6 | 69.6 | 226.0 | 10.0 | 3 | 2.99 | 153.32 | 73.2 | 202.6 | 11.2 | 8 | 7.72 | 25.30 |

Inclination and declination are site mean inclination and declination on each quantity; $\alpha_{95}$ is the angle of 95% confidence about the calculated mean direction, N, number of unit vectors averaged, R, vector sum of the respective N unit vectors, and k, best estimate of Fisher's precision parameter [Fisher, 1953].

$(K_1/K_2)/(K_2/K_3)$, where $K_1$, $K_2$, and $K_3$ are the average maximum, intermediate, and minimum susceptibility magnitudes, respectively. The ellipsoids do not become progressively more oblate or prolate with increasing strain. Instead, the points are evenly distributed about and close to the $K = 1$ line, which separates prolate (above the line) and oblate (below the line) susceptibility ellipsoids. However, the distance from the origin does tend to increase with increasing strain, showing that the anisotropy does increase with increasing strain.

The directional coincidence of the magnetic and strain fabric elements suggests that the magnitudes of the strain and AMS ellipsoid axes should be simply related. Previous studies have reported both power relationships and logarithmic relationships between strain and AMS magnitude [Rathore, 1980; Wood et al., 1976; Kligfield et al., 1981]. In the Santa Catalina sites, the shape of

the magnetic susceptibility ellipsoid does not change systematically with increasing strain, nor is there a direct correlation between the shape of the AMS ellipsoid and the shape of the corresponding strain ellipsoid for each site. However, as shown in Figure 7, the following logarithmic relationship between strain and principal susceptibility difference magnitudes (similar to what Kligfield et al. [1981] observed) is observed:

$$\Delta K_i = (0.133)\epsilon_i, \quad i = 1, 2, 3 \tag{3}$$

where

$$\Delta K_i = (K_i - \overline{K})/\overline{K}, \quad i = 1, 2, 3, \tag{4}$$

$$\overline{K} = (K_1 + K_2 + K_3)/3 \tag{5}$$

and

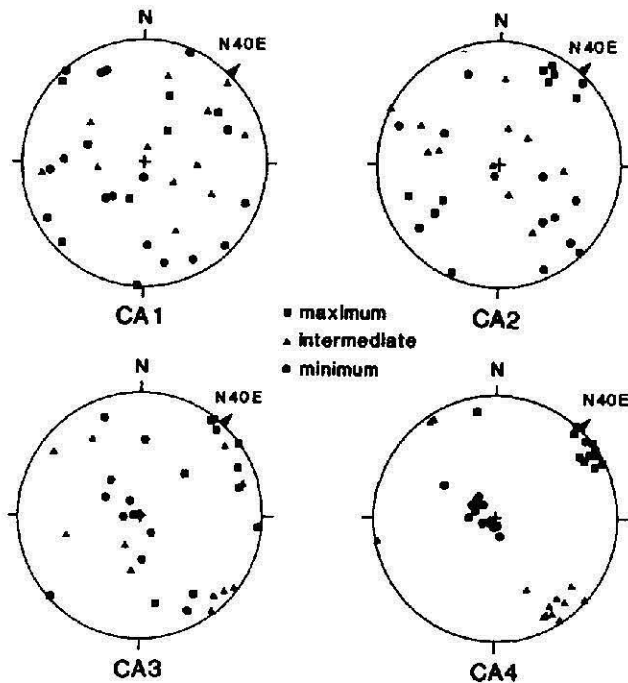$$\epsilon_i = \ln(1 + e_i), \quad i = 1, 2, 3 \tag{6}$$

Fig. 4. Lower hemisphere equal-area projections showing the distribution of principal susceptibility axes for four sites. Site CA1 is unstrained. Strain increases progressively from CA2 to CA4.

$K_1$, $K_2$, and $K_3$ correspond to the maximum, intermediate, and minimum susceptibility magnitudes, respectively, and $e_1$, $e_2$, and $e_3$ correspond to the maximum, intermediate, and minimum finite strain magnitudes, respectively.

$\Delta K_1$, $\Delta K_2$, and $\Delta K_3$ were determined independently for each sample. Thus the fact that the line in Figure 7 passes through the origin and has the same slope in the first and third quadrants is significant and is not an artifact of the calculations. Because the deformation is plane strain deformation, $\epsilon_2$ equals zero, and $Z = 1/X$. Because $\Delta K_i$ is a linear function of $\epsilon_i$, these conditions of deformation imply that $\Delta K_2$ should equal zero and $\Delta K_3$ should equal $1/\Delta K_1$ in each of the deformed samples. The intercept (0, 0) and the equivalent slopes in the two quadrants reflect the fact that $\Delta K_2$ is approximately zero and $\Delta K_3$ is approximately $1/\Delta K_1$ in each sample.

Microscope analyses, as well as thermal demagnetization of isothermal remanent magnetization acquisition and Curie temperature analyses, show that magnetite is the dominant ferromagnetic phase. In the undeformed granite, magnetite is the only optically visible magnetic phase. Grain diameters range in size from less than 10 $\mu$m to greater than 1000 $\mu$m. Eighty percent of the grains are elongate, with an average length-to-width ratio of 2.4:1. Hence the individual magnetite grains have a strong shape anisotropy due to their elongation. Magnetite

occurs both as inclusions in the basal cleavage planes of mica grains (Figure 8a) and as individual grains (Figure 8b). Thin sections from the strained sites indicate that 70-100 percent of the magnetic minerals are magnetite and 0-30 percent are hematite. The magnetite occurs both as elongate porphyroclasts and inclusions in mica grains. The hematite occurs as partial replacement of and/or pseudomorphs after magnetite. On the basis of thin-section measurements of 250 grains, the length-to-width ratio of the elongate magnetite grains may increase from 2.4:1 in the undeformed granite to 3.5-3.75:1 in the strained granite. Alternatively, this observed increase may be a sampling artifact.

The development of preferred orientations of the magnetite grains was examined by measuring the orientations of the long axes of magnetite grains with respect to the foliation plane (XY plane) and with respect to the lineation direction (X) (see Figure 9). With increasing strain, elongate magnetite grains are (1) rotated into the foliation plane (Figures 8b and 8c and Figures 9d and 9e); and (2) rotated toward the mylonitic lineation direction (Figures 9b-9e). The development of preferred alignment is predominantly accomplished by rotation of mica cleavage planes into the mylonitic foliation. Since much of the elongate magnetite is incorporated within the mica cleavage planes, rotation of the mica will also rotate the included magnetite into the mylonitic fabric (see Figure 8c). These observations suggest that in the Santa Catalina Mountains mylonite zone the
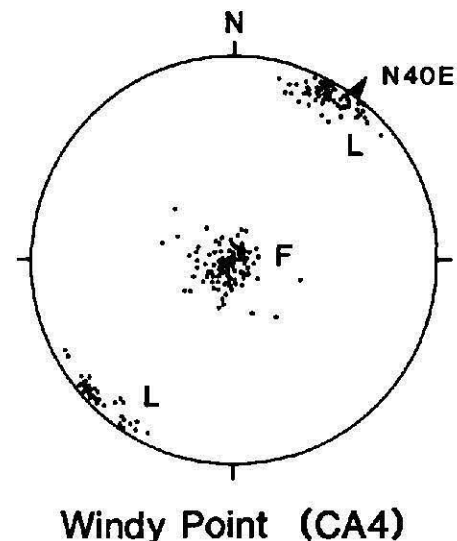


**Windy Point (CA4)**

Fig. 5. Projection of petrofabric lineation direction (L) and poles to petrofabric foliation (F) at site CA4. The lineation and poles to foliation coincide, respectively, with the maximum and minimum susceptibility axes for this sampling site (Figure 4).

development of AMS was controlled by the reorientation of originally randomly oriented elongate magnetite grains (Figure 8a) into the mylonitic foliation and lineation directions with increasing strain.

## Pinaleno Mountains

The AMS results from the Pinaleno Mountains are significantly different from those in the Catalinas. In the Pinaleno samples, the orientations of the AMS ellipsoid axes are not directly related to the petrofabric elements. Site PN1 (Figure 10a), which is petrographically essentially undeformed, shows a pronounced magnetic fabric. The three principal susceptibilities are distinctly isolated from each other, and they essentially parallel the megascopic fabric elements of the mylonite zone (Figure 11), with maximum susceptibility parallel to the mylonitic lineation direction and minimum susceptibility parallel to the mylonitic foliation pole (Figure 11). In sites PN5, PN2, and PN3 (Figure 10), the minimum susceptibility axis does coincide with the pole to the mylonitic foliation, but the intermediate and maximum susceptibility axes show no systematic relation to the mylonitic



Fig. 7. Correlation of principal susceptibility ⸱difference (equation (4)) and principal finite strain (equation (6)) in the mylonite zone of the Santa Catalina mountains. Circles and squares represent minimum and maximum strains and susceptibilities, respectively. The line has a correlation coefficient of 0.90.

lineation, which plunges gently to the northeast (N40°E). Thus, as strain increases in the Pinaleno mylonite zone, initially well-developed magnetic susceptibility ellipsoids appear to become less developed. These results are in direct contrast to those from the Santa Catalina Mountains, where a progressive change from isotropic magnetic susceptibility to anisotropic magnetic susceptibility with increasing strain is observed.

In addition, no quantifiable relationship between the shapes of the AMS and strain ellipsoids is evident, and the logarithmic relationship between susceptibility difference and finite strain found in the Santa Catalina Mountains does not apply to the Pinaleno results. The AMS ellipsoid shapes are oblate with the exception of the highest strained site (PN3), which displays a prolate ellipsoid shape (see Figure 6, open circles).

The magnetic minerals of the Pinaleno Mountains samples consist of about 85 percent magnetite and 15 percent hematite. Individual grain sizes range from less than 10 $\mu$m to greater than 1000 $\mu$m. In the unstrained granite, 60-70 percent of the magnetite grains are equant, and the remaining are randomly oriented elongate grains with average length-to-width ratios of 3.0:1.0. Magnetite is not associated with mica grains as it is in the Santa Catalina granites. J. M. Crespi and P. A. Weisse (work in preparation, 1987) report that secondary hematite is commonly associated with biotite and magnetite in the Pinaleno rocks.

In the deformed granite, magnetite is rotated into the plane of foliation, but it is not distinctly elongated parallel or perpendicular to the mylonitic
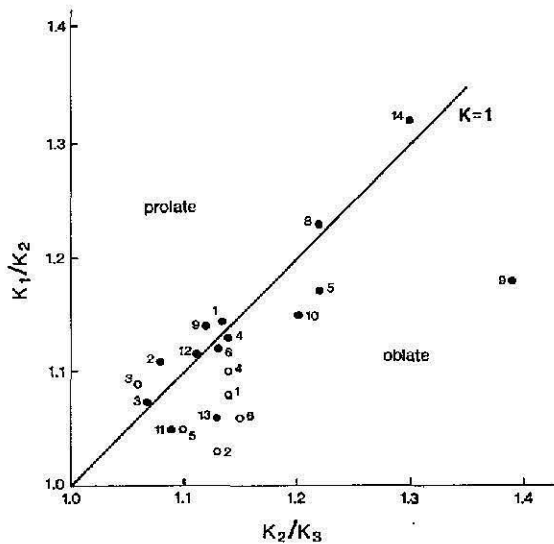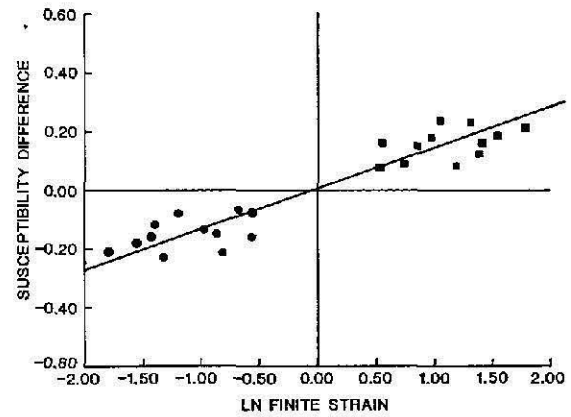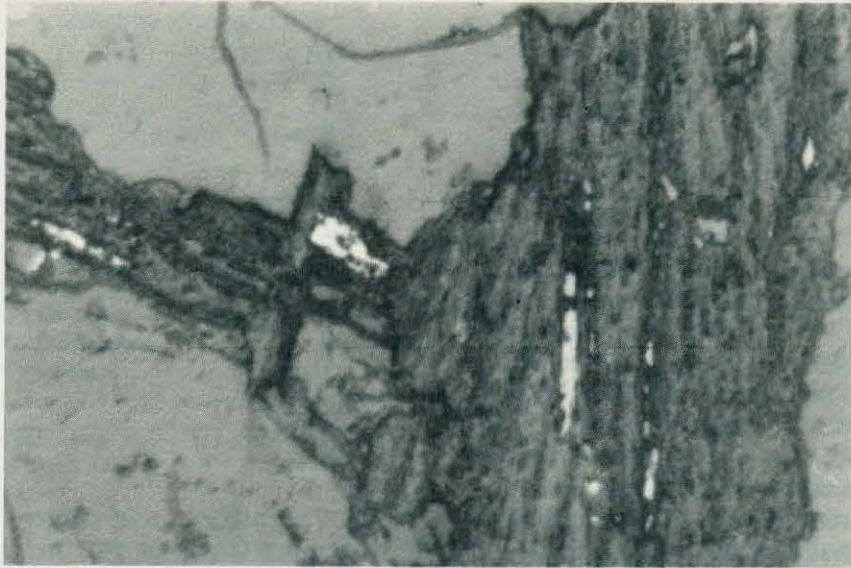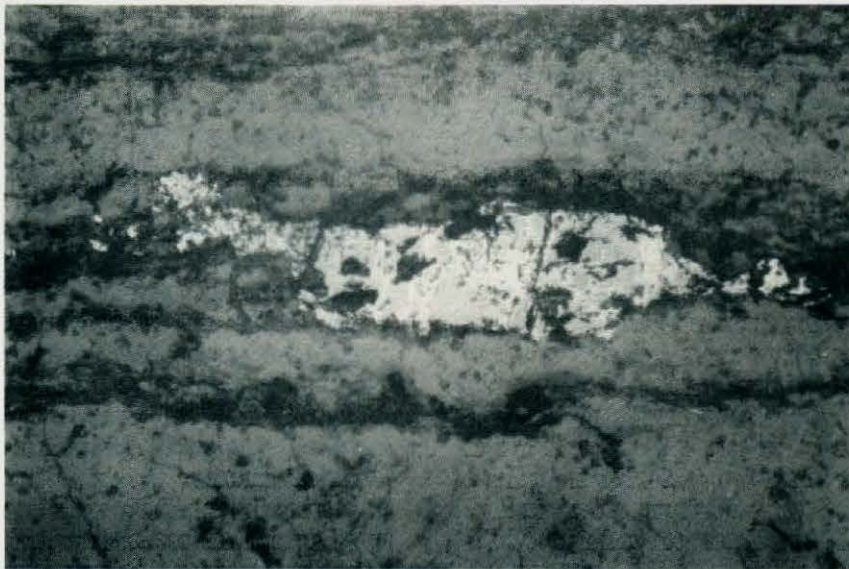


Fig. 6. Magnetic anisotropy plot showing the shape of susceptibility ellipsoids for the Santa Catalina Mountains (solid circles) and Pinaleno Mountains (open circles). Site numbers are indicated. K values greater than 1 represent prolate ellipsoids, while K values less than 1 represent oblate ellipsoids. K values for the Santa Catalina Mountains are approximately equal to 1, while K values for the Pinaleno Mountains are less than 1 at five of six sites. See Table 1 for corresponding finite strain ($\gamma$) and anisotropy factor (K) values of individual sites.

a)



b)

Fig. 8. Reflected-light photomicrographs from field-oriented Santa Catalina Mountains samples showing (a) magnetite within the basal cleavage planes of biotite in unstrained granite (field width is 0.35mm.), (b) magnetite incorporated in quartz ribbons which define the foliation planes, and (c) magnetite incorporated in the cleavage planes of mica grains which define the mylonitic foliation. For both (b) and (c), field width is 0.7 mm. Both (b) and (c) parallel the XZ strain plane, with the long dimensions of the photos parallel to X.

lineation. In thin sections oriented perpendicular to foliation and parallel to lineation, approximately 50 percent of the magnetite occurs as equant grains, and 50 percent occurs as strings subparallel to foliation but composed of equant grains. These observations are consistent with those of J. M. Crespi and P. A. Weisse (work in preparation), who report that in addition, hematite basal pinacoids

c)

Fig. 8. (continued)

and hematite strings are oriented subparallel to the trace of the mylonitic foliation. They suggest that the observed alignment of hematite results from the mimetic recrystallization of hematite during the oxidation of biotite.

In planes parallel to foliation, magnetite occurs as equant grains with no obvious elongation. In planes perpendicular to foliation and lineation, magnetite occurs as equant grains, and as grains slightly elongated parallel to the foliation. Thus the maximum susceptibility axes do not reflect the mylonitic lineation direction, but the minimum susceptibility axes do parallel the pole to the mylonitic foliation plane.

## DISCUSSION AND CONCLUSIONS

The anisotropy of magnetic susceptibility is an excellent indicator of strain in the Santa Catalina mylonite zone. The orientations of maximum, intermediate, and minimum susceptibilities coincide with the orientations of the principal strains, X, Y, and Z, respectively. Quantitatively, strain and AMS are logarithmically related by the magnitudes of finite strain and susceptibility difference. However, this relationship is at least in part a function of the shape and occurrence of the original magnetic minerals in the zone and is therefore not universal.

Thin sections from the Santa Catalina Mountains indicate that magnetite occurs primarily as uniformly distributed, randomly oriented elongate inclusions within mica grains in the undeformed granite. In the deformed state the long axes become increasingly aligned parallel to the mylonitic lineation direction (X) and are rotated into the mylonitic foliation plane (XY-plane) as mica cleavage planes are rotated into the foliation with increasing strain. As a result of these rotations, a well-defined magnetic fabric develops parallel to the megascopic fabric. However, alignment of principal susceptibilities with X, Y, and Z does not continue to increase markedly in moderately to highly strained samples.

In the Pinaleno Mountains mylonite zone the minimum susceptibility direction coincides with the mylonitic foliation pole (Z), but maximum and intermediate susceptibility directions do not coincide with X and Y, respectively. In addition, no logarithmic or other quantifiable relationship between AMS and strain magnitudes is evident.

Most of the magnetite grains in the Pinaleno mylonite zone are equant rather than elongate. Grains that are elongate are rotated into the mylonitic foliation plane with increasing strain, giving rise to the predominantly oblate AMS ellipsoid shapes seen in Figure 6. However, no preferential orientation of long axes within that plane is observed. Magnetite does not occur as mica cleavage plane inclusions as it does in the Santa Catalina Mountains. Therefore the mechanism of passively rotating elongate magnetite grains, embedded in mica grains, into the megascopic fabric directions does not operate in the Pinaleno Mountains.

The above observations suggest that the development of AMS is primarily influenced by the passive rotation of elongate ferromagnetic grains
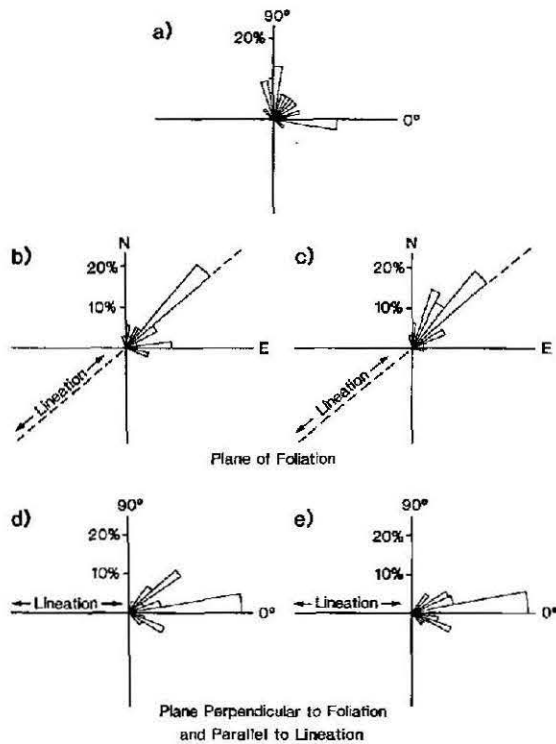
Fig. 9. Rose diagrams showing the distribution of the long axes of elongate magnetite grains in undeformed granite (a) and deformed granite (b - e) in the Santa Catalina Mountains. Figures 9b and 9d represent a relatively low strain ($\gamma = 1.1$; site CA3), and Figures 9c and 9e represent a relatively high strain ($\gamma = 5.8$; site CA8). In Figures 9b and 9c, 61% and 75% of the long axes, respectively, fall within $\pm$ 30° of the petrographic lineation direction. In Figures 9d and 9e, 64% and 80% of the long axes, respectively, fall within $\pm$ 30° of the petrographic lineation.

as a function of strain. In the Santa Catalina Mountains, where magnetite grains are initially elongate and randomly oriented, AMS is a direct function of strain magnitude. In this case, the original AMS ellipsoid shape is spherical, or isotropic. Thus, as strain increases, the initially spherical AMS ellipsoid becomes increasingly ellipsoidal and reflects the strain magnitude. In the Pinaleno Mountains, in contrast, AMS is not a simple function of strain. In this case, the original magnetite grains are not elongate, and the AMS ellipsoid is not initially spherical (Figure 10a). Therefore the final AMS ellipsoid shape is not a direct function of strain but rather may be some function of the original AMS ellipsoid shape and strain. In particular, the final AMS tensor may be the product of the original AMS tensor and the imposed deformation matrix.

Development of AMS by passive rotation of ferromagnetic grains is limited in part by the degree to which elongate grains can be aligned.

As alignment approaches a maximum degree, the degree of AMS also approaches a limit. Lowrie et al. [1986] have reported that AMS develops quickly at low strains but saturates rapidly and cannot exceed a finite value. In the Santa Catalina Mountains a magnetic fabric develops rapidly at low strains. However, as strain increases, the AMS ellipsoid shape does not change markedly. This suggests that alignment of principal susceptibility axes with X, Y, and Z occurs rapidly at low strains but does not increase or change significantly with further strain increases. Thus there are limits on the degree to which strain can be determined from AMS data.

The effects of strain-related recrystallization on the development of AMS in the mylonite zones appear to be relatively insignificant. The deformational histories of the two zones are very similar; both have been subjected to plane strain, simple shear at similar (greenschist facies) pressure and temperature conditions. Therefore grain recrystallization and shape change effects due to strain should be similar in the two zones. Since the AMS signature is undeniably different in the
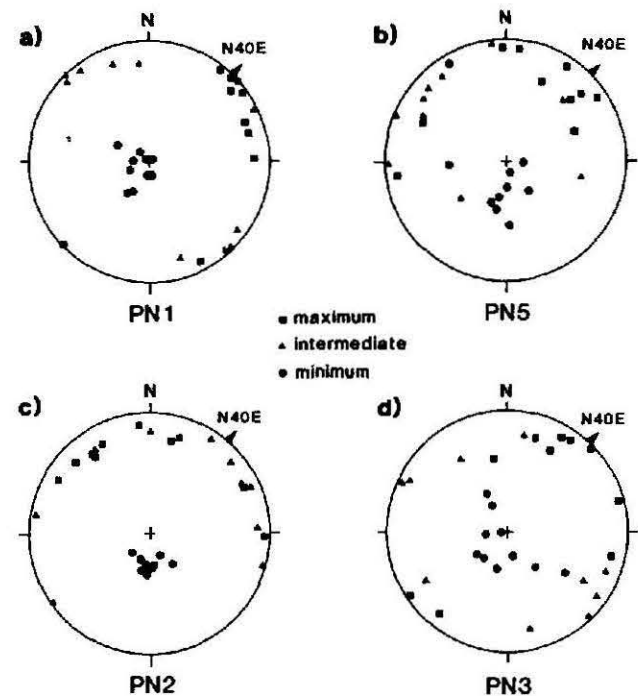


Fig. 10. Lower hemisphere equal-area projections showing the distribution of principal susceptibility axes for four sites in the Pinaleno Mountains. Strain increases progressively from Figures 10a to 10d, and Figure 10a is essentially undeformed. Minimum susceptibility axes generally represent the pole to mylonitic foliation, but maximum and intermediate susceptibilities are not systematically aligned; they show no correspondence to the mylonitic lineation.

two zones, strain-related (dynamic) recrystallization and shape change do not appear to be dominant factors controlling AMS development.

The effects of thermal or hydrothermal recrystallization may be significant, however. J. M. Crespi and P. A. Weisse (work in preparation, 1987) suggest that the observed oblate magnetic fabric in the Pinaleno Mountains mylonite zone could be the result of synkinematic to postkinematic recrystallization of hematite. This secondary hematite cannot record the entire strain history, but it reflects the planar fabric already developed in the rock. These results highlight the importance of microscopic observations in the interpretation of AMS data.

In general, the results indicate that oblate- or prolate-shaped AMS ellipsoids are not necessarily reflections of oblate or prolate strain ellipsoids, respectively. For instance, in the Pinaleno Mountains, K = 1 for strain ellipsoids, but K is consistently less than 1 for AMS ellipsoids.

Goldstein and Brown [1986] explain the common occurrence of oblate AMS ellipsoids in mylonite zones by suggesting that these zones may be subjected to large flattening strains perpendicular to the zone, yielding oblate strain ellipsoids. The strain analyses of the Pinaleno zone, however, show that the strain ellipsoid within the zone is not oblate. Thus the oblate AMS ellipsoid in this case is not related to an oblate strain ellipsoid.

It appears that the magnetic fabric in the Santa Catalina and Pinaleno mylonites is predominantly controlled by the alignment and orientation of elongate magnetite grains with respect to the petrofabric elements. Grain shape change, development of strings of magnetite grains, and secondary hematite recrystallization probably contribute to the magnetic anisotropy in the Pinaleno Mountains (J. M. Crespi and P. A. Weisse, work in preparation, 1987). However, alignment of elongate magnetite grains during ductile deformation in the Santa Catalina Mountains is clearly the dominant mechanism of AMS development in that mylonite zone. Therefore, despite the similar deformational history, structure, and bulk mineralogy of these two mylonite zones, they display remarkably different AMS patterns because of differences in shape, orientation, and host mineral occurrence of magnetic minerals within the two mylonite zones.
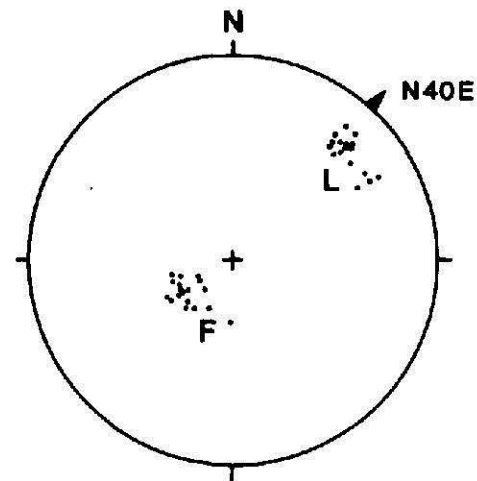
## Pinaleno Mountains

Fig. 11. Projection of petrofabric lineation direction (L) and poles to petrofabric foliation (F) in the Pinaleno mylonite zone.

## REFERENCES

Crittenden, M. D., Jr., P. J. Coney, and G. H. Davis (eds.), Cordilleran Metamorphic Core Complexes, *Mem. Geol. Soc. Am. 153*, 1 490, 1980.

Davis, G. H., and P. J. Coney, Geological development of the Cordilleran metamorphic core complexes, *Geology, 7*, 120–124, 1979.

Fisher, R. A., Dispersion on a sphere, *Proc. R. Soc. London, 7*, 295–305, 1953.

Goldstein, A. G., Magnetic susceptibility anisotropy of mylonites from the Lake Char mylonite zone, southeastern New England, *Tectonophysics, 66*, 197–211, 1980.

Goldstein, A. G., and L. L. Brown, Magnetic susceptibility anisotropy of mylonites from the Brevard zone, North Carolina, U.S.A., *Phys. Earth Planet. Inter.*, in press, 1986.

Graham, J. W., Significance of magnetic anisotropy in Applachian sedimentary rocks, in *The Earth Beneath the Continents, Geophys. Monogr. Ser.*, vol. 10, edited by J. S. Steinhart and T. J. Smith, pp. 627–648, AGU, Washington D.C., 1966.

Holt, W. E., C. G. Chase, and T. C. Wallace, Crustal structure from three-dimensional gravity modeling of a metamorphic core complex: A

model for uplift, Santa Catalina-Rincon mountains, Arizona, *Geology*, *14*, 927–930, 1986.

Hrouda, F., Magnetic anisotropy of rocks and its application in geology and geophysics, *Geophys. Surv.*, *5*, 37–82, 1982.

Kligfield, R., W. Lowrie, and I. W. D. Dalziel, Magnetic susceptibility anisotropy as a strain indicator in the Sudbury Basin, Ontario, *Tectonophysics*, *40*, 287–308, 1977.

Kligfield, R., W. H. Owens, and W. Lowrie, Magnetic susceptibility anisotropy, strain and progressive deformation in Permian sediments from the Maritime Alps (France), *Earth Planet. Sci. Lett.*, *55*, 181–189, 1981.

Kligfield, R., W. Lowrie, and O. A. Pfiffner, Magnetic properties of deformed oolites from the Swiss Alps: The correlation of magnetic anisotropy and strain, *Eclogae Geol. Helv.*, *75*, 127–157, 1982.

Kligfield, R., W. Lowrie, A. M. Hirt, and A. W. B. Siddans, Effect of progressive deformation on remanent magnetization of Permian redbeds from the Alpes Maritimes (France), *Tectonophysics*, *97*, 59–85, 1983.

Lowrie, W., A. M. Hirt, and R. Kligfield, Effects of tectonic deformation on the remanent magnetization of rocks, *Tectonics*, *5*, 713–722, 1986.

Naruk, S. J., Strain and displacement across the Pinaleno mountains shear zone, Arizona, USA, *J. Struct. Geol.*, *8*, 35–46, 1986a.

Naruk, S. J., Finite strains and mylonitic fabrics in the Santa Catalina core complex, southern Arizona, *Geol. Soc. Am. Abstr. Programs*, *18*, 163, 1986b.

Naruk, S. J., Kinematic significance of mylonitic foliation, Ph.D. dissertation, Univ. of Arizona, Arizona, 1987a.

Naruk, S. J., Displacement calculations across a metamorphic core complex mylonite zone: Pinaleno Mountains, southeastern Arizona, *Geology*, *15*, 656-660, 1987b.

Ramsay, J. G., *Folding and Fracturing of Rocks*, 568 pp., McGraw Hill, New York, 1967.

Ramsay, J. G., and R. H. Graham, Strain variation in shear belts, *Can. J. Earth Sci.*, *7*, 786–813, 1970.

Ramsay, J. G., and M. Huber, *Techniques of Modern Structural Geology*, 307 pp., Academic, Orlando, Fla., 1983.

Rathore, J. S., The magnetic fabric of some slates from the Borrowdale volcanic group in the English Lake District and their correlation with strain, *Tectonophysics*, *67*, 207–220, 1980.

Rathore, J. S., Some magnetic fabric characteristics of sheared zones, *Geodynamics*, *2*, 291–301, 1985.

Rathore, J. S., G. Courrioux, and P. Choukroune, Study of ductile shear zones (Galacia, Spain) using texture goniometry and magnetic fabric methods, *Tectonophysics*, *98*, 87–109, 1983.

Wood, D., G. Oertel, J. Singh, and H. Bennett, Strain and anisotropy in rocks, *Philos. Trans. R. Soc. London, Ser. A*, *283*, 27–42, 1976.

---

R. F. Butler, G. J. Calderone, and A. S. Ruf, Department of Geosciences, University of Arizona, Tucson, AZ 85721.

S. J. Naruk, Shell Western E & P Inc., P.O. Box 527, Houston, TX 77001.